Journal of Porous Media, 23(1):11–26 (2020)

IMPACT OF NON-DARCY MEDIUM ON MIXED CONVECTIVE FLOW TOWARDS A PLATE CONTAINING MICROPOLAR WATER-BASED TiO_2 NANOMATERIAL WITH ENTROPY GENERATION

A. Zaib,[1,*] R.U. Haq,[2] M. Sheikholeslami,[3] A.J. Chamkha,[4] & M.M. Rashidi[5]

[1]*Department of Mathematical Sciences, Federal Urdu University of Arts, Science, & Technology, Gulshan-e-Iqbal Karachi-75300, Pakistan*

[2]*Department of Electrical Engineering, Bahria University Islamabad, Islamabad, Pakistan*

[3]*Department of Mechanical Engineering, Babol University of Technology, Babol, Islamic Republic of Iran*

[4]*Mechanical Engineering Department, Prince Mohammad Bin Fahd University, Al-Khobar 31952, Saudi Arabia*

[5]*Department of Civil Engineering, School of Engineering, University of Birmingham, Birmingham, UK*

*Address all correspondence to: A. Zaib, Department of Mathematical Sciences, Federal Urdu University of Arts, Science, & Technology, Gulshan-e-Iqbal Karachi-75300, Pakistan, E-mail: zaib20042002@yahoo.com

Original Manuscript Submitted: 8/20/2018; Final Draft Received: 2/5/2019

The theme of current research is to explore the impact of entropy generation on mixed convective flow of micropolar fluid containing water-based TiO_2 nanomaterial toward a vertical surface in a non-Darcy porous medium. The results are confined for opposing and assisting flows. Similarity equations are achieved and then worked out numerically by the Keller box technique. The impacts of substantial parameters on temperature distribution, velocity profile, and microrotation velocity, together with the Nusselt number and the skin friction, are illustrated with the help of graphs. Two solutions are achieved in opposing flow while the solution is unique in assisting flow. It is also observed that the separation of boundary layer accelerates due to volume fraction and delays due to micropolar parameter.

KEY WORDS: *micropolar fluid, mix convection, entropy generation, non-Darcy medium, TiO_2 nanomaterial*

1. INTRODUCTION

In recent times, fluids containing nanometer sized particles, nanofluids, have come into use. Nanofluids are utilized because dispersing particles into base liquids can enhance the fluid's thermal conductivity. These particles are solid in environment and have no additional barriers similar to erosion and droplet of extra pressure, etc. The presence of particles would improve the thermal conductivity of liquids in the heat transfer processes that remain essential in a number of engineering applications involving electronics, nuclear reactors, foodstuffs, and biomedicine. Many scientists and researchers have studied the nanofluid rheology. Initial studies by Choi (1995) described the concept of nanofluids. He showed experimentally that the properties of thermal characteristics can be increased by dispersing nanoparticles into regular liquids. Wang et al. (1999) studied the characteristics of nanoparticles involving boundary layering and grouping of fluid particles that might suggest fast heat transfer. Khan and Pop (2010) presented the flow containing nanoliquid past an elongating sheet. The numerical solution of flow involving nanoliquid from an elongating

convectively heated surface was developed by Makinde and Aziz (2011). Sandeep et al. (2015) discussed the unsteady flow of magnetohydrodynamic (MHD) thermophoretic nanoliquid from a stretched sheet containing some physical aspects. Makinde et al. (2016) scrutinized the impact of magnetic effect on radiative flow holding nanoparticles over a radial heated stretched surface with variable viscosity. Rashid et al. (2017) explored the effect of variable temperature on flow of water-based alumina and copper nanoparticles from a shrinking surface through thermal radiation. Umavathi and Sasso (2018) discussed the impact of variable properties on free convective flow comprising nanofluid through a duct embedded in porous medium. The impact of bioconvection flow comprising nanoliquids driven from a wedge embedded in Darcy–Brinkman porous medium with convective boundary condition was discussed by Zaib et al. (2018). Recently, Iqbal et al. (2019) explored the behavior of slip flow involving ferroliquid from a stretching surface with viscous dissipation and thermal radiation.

The influences of non-Newtonian liquids are cause of motivation to researchers and engineers in modern times. Such liquids commonly arise in different processes, for instance printing of ink jet coating, process of polymer, geological flows, suspensions of colloidal flows, fluid crystals, production of mayonnaise, and numerous other processes. Therefore, this developed to be a topic of significance to distinguish the flow performances of such types of liquids. Micropolar liquids are among the considerable non-Newtonian liquids in the microscale. Theory of micropolar liquid is a class of liquids that displays certain characters of microscopic occurring from the micro rotation and local structure of the liquid elements. These liquids involve diluting suspensions of rigid macromolecules through individual movements that carry body moments and stress and are exaggerated by the spin inertia. Eringen (1966) developed the theory that a compact class of fluids which shows certain characteristics on the microscale occurring from fluid elements' local structure and the microrotation. Recent studies showed the importance of micropolar fluid. For instance, Saleh et al. (2017), Waqas et al. (2017), and Hussanan et al. (2017) discussed the influence of micropolar fluid in certain aspects. In recent times, a new era in research has begun by adding the nanoliquid in micropolar fluid. Das and Duari (2017) obtained the numerical results of the flow from a stretched surface containing micropolar nanomaterial with chemical reaction. Hsiao (2017) extended this problem by involving the combined effects of MHD and viscous dissipation. Hussanan et al. (2018) considered the micropolar model under the effect of magnetite ferrofluid past a stretched/shrinking sheet with effective thermal conductivity. Recently, Yasmin et al. (2019) discussed the influence of MHD flow with heat transfer comprising micropolar fluid in porous channel with viscous dissipation.

Darcy flow is suitable in a porous medium at very small Reynolds number or having very low permeability. In contrast to Darcy flow, the position of flow in non-Darcy occurs with fluid velocity and large Reynolds number in the presence of a medium. Non-Darcy flow takes place in high fluctuation wells through gas and oil production, pumping water, and waste injection of liquid. Mukhopadhyay et al. (2012) explored the impact of radiation on forced convection flow from a surface entrenched in a Darcy–Forchheimer medium. Prasad et al. (2014) scrutinized the influence of non-Darcy flow of Jeffrey's fluid toward a vertical permeable plate and obtained the numerical solution via Keller box technique. The electric conducting fluid from a stretched surface filled with non-Darcy porous medium was investigated numerically by Gireesha et al. (2015). Mabood et al. (2016) discussed the impacts of nonuniform source/sink and MHD on flow of a micropolar fluid in non-Darcy porous medium. Hayat et al. (2017) envisaged the influences of Joule heating and thermal radiation on Darcy–Forchheimer flow containing copper/silver nanoparticles between two stretched and rotated disks. Recently, Bakar et al. (2018) scrutinized the impact of suction on forced convective flow through a shrinking surface in Darcy porous medium with thermal radiation.

Entropy generation has been utilized to measure the importance of irreversibility connected to friction, heat transfer, and additional nonideal processes in thermal systems. To enhance the presentation of any heat transfer procedure, entropy generation has been widely used. Spasojević et al. (2010) used minimization of entropy generation in column of diabetic refinement through trays, where they considered the exchanged heat as a control variable rather than temperature. Butt and Ali (2014) explored the influences of radiation and entropy generation on hydromagnetic free convective flow toward a vertical sheet entrenched in porous medium. A relaxation spectral method has been used by Shateyi et al. (2015) to investigate the entropy generation on magnetic flow of a Maxwell liquid past a stretched sheet. Zaib et al. (2017) scrutinized the impact of activation energy on electrical conducting Casson nanomaterial from a wedge with entropy generation and binary chemical reaction. Khan et al. (2018) discussed the importance of entropy generation on flow owing to a stretched rotating disk. Recently, Sreenadh et al. (2018) explored the impacts of MHD and heat source on free convective flow via a deformable permeable layer with entropy generation.

The addition of micropolar liquid with TiO_2-water nanomaterial presents a more complex mixture compared to regular nanoliquids. This investigation begins a novel era for researchers to discover the characteristics of micropolar nanofluid in non-Darcy porous media. Therefore, we investigated the mixed convective flow containing micropolar TiO_2-water nanomaterial past a vertical plate in a non-Darcy porous medium with entropy generation. Similarity equations were developed and obtained dual numerical solutions via the Keller box technique. The influences of the substantial parameters are presented in detail using tables and graphs.

2. PROBLEM FORMULATION

Consider a steady mixed convection flow of micropolar liquid holding TiO_2 nanomaterial near a stagnation point toward a vertical surface in non-Darcy porous medium with entropy generation. A porous medium is filled with incompressible fluid, and that medium is described by the non-Darcy relation. The physical diagram is presented in Fig. 1. We presume that the free stream velocity is $\breve{u}_e(\breve{x}) = c\breve{x}$ and wall temperature $\breve{T}_w(\breve{x}) = \breve{T}_\infty + b\breve{x}$ vary linearly, where c and b are positive constants and $\breve{T}_\infty$ is ambient temperature. The governing equations under these assumptions through the usual boundary layer and the Boussinesq approximation are written as follows (Hayat et al., 2017; Hussanan et al., 2018):

$$\frac{\partial \breve{u}}{\partial \breve{x}} + \frac{\partial \breve{v}}{\partial \breve{y}} = 0, \tag{1}$$

$$\begin{aligned}\breve{u}\frac{\partial \breve{u}}{\partial \breve{x}} + \breve{v}\frac{\partial \breve{u}}{\partial \breve{y}} - \breve{u}_e\frac{d\breve{u}_e}{d\breve{x}} &= \frac{1}{\breve{\rho}_{nf}}\left(\breve{\mu}_{nf} + \breve{\kappa}\right)\frac{\partial^2 \breve{u}}{\partial \breve{y}^2} + \frac{\breve{\kappa}}{\breve{\rho}_{nf}}\frac{\partial \breve{N}}{\partial \breve{y}} - \frac{\breve{\mu}_{nf}}{\breve{\rho}_{nf}\breve{k}_1}\left(\breve{u} - \breve{u}_e\right) \\ &- \frac{c_b}{\sqrt{\breve{k}_1}}\left(\breve{u}^2 - \breve{u}_e^2\right) + \frac{g\left(\rho\beta\right)_{nf}}{\breve{\rho}_{nf}}\left(\breve{T} - \breve{T}_\infty\right),\end{aligned} \tag{2}$$

$$\breve{u}\frac{\partial \breve{N}}{\partial \breve{x}} + \breve{v}\frac{\partial \breve{N}}{\partial \breve{y}} = \frac{\breve{\gamma}_{nf}}{\breve{\rho}_{nf}j}\frac{\partial^2 \breve{N}}{\partial \breve{y}^2} - \frac{\breve{\kappa}}{\breve{\rho}_{nf}j}\left(2\breve{N} + \frac{\partial \breve{u}}{\partial \breve{y}}\right), \tag{3}$$

$$\breve{u}\frac{\partial \breve{T}}{\partial \breve{x}} + \breve{v}\frac{\partial \breve{T}}{\partial \breve{y}} = \breve{\alpha}_{nf}\frac{\partial^2 \breve{T}}{\partial \breve{y}^2}, \tag{4}$$

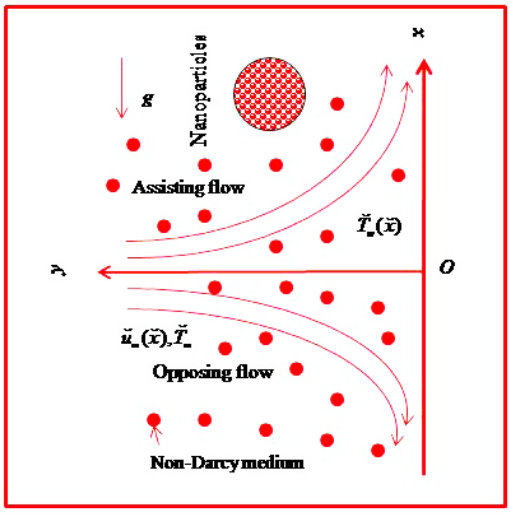

FIG. 1: Physical diagram of the problem

The physical boundary conditions are

$$\begin{aligned} &\breve{u}=0, \quad \breve{N}=-\breve{n}\frac{\partial \breve{u}}{\partial \breve{y}}, \quad \breve{v}=0, \quad \breve{T}=\breve{T}_w(\breve{x}) \quad \text{at} \quad \breve{y}=0, \\ &\breve{u}\to \breve{u}_e(\breve{x}), \quad \breve{T}\to \breve{T}_\infty, \quad \breve{N}\to 0 \quad \text{as} \quad \breve{y}\to\infty, \end{aligned} \tag{5}$$

where $\breve{v}$, $\breve{u}$ are the components of velocity in the $\breve{x}$- and $\breve{y}$-directions; $\breve{\rho}_{nf}$, $\breve{\mu}_{nf}$, $\breve{\kappa}$, c_b, $\breve{k}_1$, g, and β_{nf} are the fluid density, fluid dynamic viscosity, vortex viscosity, Forchheimer coefficient, permeability parameter, acceleration caused by gravity, and nanofluid thermal expansion, respectively; $\breve{N}$, $\breve{T}$, $\breve{\gamma}_{nf}$, $\breve{\alpha}_{nf}$, j, and $\breve{n}$ are microrotation vector, temperature, spin gradient viscosity, thermal diffusivity, microinertia density, and microgyration parameter, respectively. It is well known that the microgyration parameter varies as $0 \le \breve{n} \le 1$, where $\breve{n}=0$ represents strong concentration, for $\breve{n}=0.5$ signifies as weak concentration and $\breve{n}=1$ indicates turbulent flow.

The values of $\breve{\rho}_{nf}$, $\breve{\alpha}_{nf}$, $(\breve{\rho}\breve{c}_p)_{nf}$, $\breve{\mu}_{nf}$, $\breve{k}_{nf}/\breve{k}_f$, $\breve{\gamma}_{nf}$, and $(\rho\beta)_{nf}$ are classified as follows (Rashid et al., 2017; Hussanan et al., 2018):

$$\begin{aligned} &\breve{\rho}_{nf}=(1-\varphi)\,\breve{\rho}_f+\varphi\breve{\rho}_s, \quad \breve{\alpha}_{nf}=\breve{k}_{nf}/\left(\breve{\rho}\breve{c}_p\right)_{nf}, \quad \left(\breve{\rho}\breve{c}_p\right)_{nf}=(1-\varphi)\left(\breve{\rho}\breve{c}_p\right)_f+\varphi\left(\breve{\rho}\breve{c}_p\right)_s, \\ &\breve{\mu}_{nf}=\frac{\breve{\mu}_f}{(1-\varphi)^{2.5}}, \quad \frac{\breve{k}_{nf}}{\breve{k}_f}=\frac{\left(\breve{k}_s+2\breve{k}_f\right)-2\varphi\left(\breve{k}_f-\breve{k}_s\right)}{\left(\breve{k}_s+2\breve{k}_f\right)+\varphi\left(\breve{k}_f-\breve{k}_s\right)}, \quad \breve{\gamma}_{nf}=\left(\breve{\mu}_{nf}+\breve{\kappa}/2\right)j, \\ &\left(\breve{\rho}\breve{\beta}\right)_{nf}=(1-\varphi)\left(\breve{\rho}\breve{\beta}\right)_f+\varphi\left(\breve{\rho}\breve{\beta}\right)_s, \end{aligned} \tag{6}$$

where φ, $\breve{k}_f$, $\breve{k}_s$, $\breve{\rho}_s$, $\breve{\rho}_f$, $\left(\breve{\rho}\breve{\beta}\right)_s$, and $\left(\breve{\rho}\breve{\beta}\right)_f$ are the volume fraction of nanoliquid, the thermal conductivity of regular liquid, thermal conductivity of nanoliquid, density of nanoliquid, density of base fluid, and coefficients of thermal expansion of nanoliquid and base fluid, respectively.

We utilize the similarity transformation:

$$\breve{u}=c\breve{x}F'(\eta), \quad \eta=y\sqrt{\frac{c}{\nu_f}}, \quad \breve{v}=-\sqrt{c\nu_f}F(\eta), \quad \breve{N}(\eta)=c\breve{x}\sqrt{\frac{c}{\nu_f}}\breve{G}, \quad \theta(\eta)=\frac{\breve{T}-\breve{T}_\infty}{\breve{T}_w-\breve{T}_\infty}. \tag{7}$$

In view of relation (7), Eqs. (2)–(6) are transmuted to

$$\begin{aligned} &\left(\frac{1+(1-\varphi)^{2.5}K}{(1-\varphi)^{2.5}}\right)F'''+\left[(1-\varphi)+\varphi\frac{\breve{\rho}_s}{\breve{\rho}_f}\right]\left(FF''-F'^2+1-\beta\left(F'^2-1\right)\right)+KG' \\ &\qquad -\frac{\alpha}{(1-\varphi)^{2.5}}\left(F'-1\right)+\lambda\left[(1-\varphi)+\varphi\frac{\left(\breve{\rho}\breve{\beta}\right)_s}{\left(\breve{\rho}\breve{\beta}\right)_f}\right]\theta=0, \end{aligned} \tag{8}$$

$$\left(\frac{2+(1-\varphi)^{2.5}K}{2(1-\varphi)^{2.5}}\right)G''+\left[(1-\varphi)+\varphi\frac{\breve{\rho}_s}{\breve{\rho}_f}\right](FG'-F'G)-K\left(2G+F''\right)=0, \tag{9}$$

$$\frac{\left(\breve{k}_s+2\breve{k}_f\right)-2\varphi\left(\breve{k}_f-\breve{k}_s\right)}{\left(\breve{k}_s+2\breve{k}_f\right)+\varphi\left(\breve{k}_f-\breve{k}_s\right)}\theta''+\mathrm{Pr}\left[(1-\varphi)+\varphi\frac{\left(\breve{\rho}\breve{c}_p\right)_s}{\left(\breve{\rho}\breve{c}_p\right)_f}\right](F\theta'-F'\theta)=0, \tag{10}$$

with the converted boundary conditions

$$\begin{aligned} &F(0)=0, \quad G(0)=-\breve{n}F''(0), \quad F'(0)=0, \quad \theta(0)=1 \\ &F'(\infty)\to 1, \quad \theta(\infty)\to 0, \quad G(\infty)\to 0. \end{aligned} \tag{11}$$

In preceding equations, the dimensionless constants micropolar parameter K, mixed convective parameter λ, inertia coefficient β, porosity parameter α, and Prandtl number Pr are described as follows:

$$K = \breve{\kappa}/\breve{\mu}_f, \quad \lambda = \breve{\beta}_f g b/c^2 = \mathrm{Gr}_x/\mathrm{Re}_x^2, \quad \mathrm{Gr}_x = g\breve{\beta}_f\left(T_w - T_\infty\right)\breve{x}^3/\nu_f^2, \quad \mathrm{Re}_x = \breve{x}\breve{u}_e(\breve{x})/\nu_f,$$
$$\beta = k\mathrm{Re}_x^{-1/2}\sqrt{c/\nu\breve{k}_1}, \quad \alpha = \breve{\mu}_f/c\breve{\rho}_f\breve{k}_1, \quad \mathrm{Pr} = \nu_f\left(\breve{\rho}\breve{c}_p\right)_f/k_f, \quad j = \nu_f/c.$$

The coefficient of skin friction and the Nusselt number are

$$C_{fx} = \frac{1}{\breve{\rho}_{nf}\breve{u}_e^2}\left[\left(\breve{\mu}_{nf} + \breve{\kappa}\right)\frac{\partial\breve{u}}{\partial\breve{y}} + \breve{\kappa}\breve{N}\right]_{\breve{y}=0}, \quad \mathrm{Nu}_x = -\frac{\breve{x}\breve{k}_{nf}}{\breve{k}_f\left(\breve{T}_w - \breve{T}_\infty\right)}\frac{\partial\breve{T}}{\partial\breve{y}}\bigg|_{\breve{y}=0}. \tag{12}$$

Using the relations (6) and (7), we obtain

$$C_{fx}\mathrm{Re}_x^{1/2} = \frac{1}{\left[\left(1-\varphi\right) + \varphi\frac{\breve{\rho}_s}{\breve{\rho}_f}\right]}\left(\frac{1 + \left(1-\varphi\right)^{2.5}\left(1-\breve{n}\right)K}{\left(1-\varphi\right)^{2.5}}\right)F''(0), \quad \mathrm{Nu}_x\mathrm{Re}_x^{-1/2} = -\frac{k_{nf}}{k_f}\theta'(0). \tag{13}$$

2.1 Entropy Generation

Entropy generation with micropolar fluid containing TiO_2 nanomaterial in a non-Darcy porous medium is engraved as

$$S_{gen}''' = \frac{\breve{k}_{nf}}{\breve{T}_\infty^2}\left(\frac{\partial\breve{T}}{\partial\breve{y}}\right)^2 + \frac{1}{\breve{T}_\infty}\left(\breve{\mu}_{nf} + \breve{\kappa}\right)\left(\frac{\partial\breve{u}}{\partial\breve{y}}\right)^2 + \frac{\breve{\mu}_{nf}}{\breve{T}_\infty\breve{k}_1}\breve{u}^2 + \frac{c_b}{\breve{T}_\infty\sqrt{\breve{k}_1}}\breve{u}^3. \tag{14}$$

Volumetric entropy number is characterized as

$$S_0''' = \frac{\breve{k}_f\left(\Delta\breve{T}\right)^2}{L^2\breve{T}_\infty^2}, \tag{15}$$

in dimensionless form

$$\begin{aligned} N_G = \frac{S_{gen}'''}{S_0'''} &= \frac{\mathrm{Re}_L\mathrm{Br}}{\Omega}\left(\frac{1 + \left(1-\varphi\right)^{2.5}K}{\left(1-\varphi\right)^{2.5}}\right)F''^2 + \frac{k_{nf}}{k_f}\mathrm{Re}_L\theta'^2 \\ &+ \frac{\mathrm{Re}_L\mathrm{Br}}{\Omega}\left(\frac{1}{\left(1-\varphi\right)^{2.5}}\right)\alpha F'^2 + \frac{1}{\beta}\frac{\mathrm{Re}_L\mathrm{Br}}{\Omega}F'^3, \end{aligned} \tag{16}$$

where $\Omega = \Delta\breve{T}/\breve{T}_\infty$, the dimensionless difference of temperature; $\mathrm{Br} = \breve{\mu}_f\breve{u}_e^2/\breve{k}_f\Delta\breve{T}$, the Brinkman number; and $\mathrm{Re}_L = cL^2/\nu_f$, the characteristic length-based Reynolds number.

3. RESULTS AND DISCUSSION

Equations (8)–(10) through boundary condition (11) are computed numerically via the Keller box technique. Here, we considered the Prandtl number $\mathrm{Pr} = 6.2$ and microgyration parameter $n = 0.5$. The thermophysical properties for regular liquids and particles are illustrated in Table 1. In Tables 2 and 3, we judged our results of $F''(0)$ and $-\theta'(0)$ with available outcomes and found them to be in tremendous agreement. Table 4 is developed to compare the evaluations between the two novel methods, namely Keller box and bvp4c methods, and found to be in excellent harmony. In addition, two-phase flow comparison is shown in Table 5 and observed to be in favorable agreement. The values of $F''(0)$ are depicted in Table 6 to compare our results with the viscous fluid model for the second solution.

TABLE 1: Thermophysical properties of base fluid and TiO_2

Material	Base fluid	TiO_2
C_p (J/kgK)	4179	686.2
ρ (kg/m^3)	997.1	4250
k (W/mK)	0.613	8.9538
$\beta \times 10^{-5}$ (1/K)	21	0.9

TABLE 2: Comparison of $F''(0)$ when $\lambda = 1$, $\varphi = 0$, $K = 0$

Pr	Lok et al. (2006)	Aman et al. (2011)	Present
0.7	1.7064	1.7063	1.7063
1	—	1.6754	1.6754
7	1.5180	1.5179	1.5179
10	—	1.4928	1.4928
20	1.4486	1.4485	1.4485
40	1.4102	1.4101	1.4101
50	—	1.3989	1.3989
60	1.3903	1.3903	1.3903
80	1.3773	1.3773	1.3776
100	1.3677	1.3680	1.3683

TABLE 3: Comparison of $-\theta'(0)$ when $\lambda = 1$, $\varphi = 0$, $K = 0$

Pr	Lok et al. (2006)	Aman et al. (2011)	Present
0.7	0.7641	0.7641	0.7641
1	—	0.8708	0.8708
7	1.7226	1.7224	1.7224
10	—	1.9446	1.9446
20	2.4577	2.4476	2.4576
40	3.1023	3.1011	3.1011
50	—	3.3415	3.3415
60	3.5560	3.5514	3.5515
80	3.9195	3.9095	3.9097
100	4.2289	4.2116	4.2120

The impact of nanoparticle volume fraction on the velocity, microrotation profiles, and temperature distribution are depicted in Figs. 2(a)–2(c), respectively. It is witnessed from Fig. 2(a) that the fluid velocity trims down as φ increases for the first solution, whereas the value grows for the second solution. Meanwhile, the profile of microrotation shows an increasing trend in both forms of solutions as portrayed in Fig. 2(b). In contrast, the temperature distribution moves up with φ for first solution and drops in second solution as illustrated in Fig. 2(c). The physical reason is that nanoparticle volume fraction of TiO_2 enhances the thermal conductivity which consequently boosts the thickness of thermal boundary layer in first solution. Alterations in the shape, size, material, and nanoparticle volume fraction permits for modification to maximize absorption of energy via the volume of fluid because the nanoparticle volume fraction depends on the size of the particle. Enhancing the volume fraction of nanoparticles results in climbing of the coefficient of heat transfer.

TABLE 4: Variation of $C_{fx}\mathrm{Re}_x^{1/2}$ and $\mathrm{Nu}_x\mathrm{Re}_x^{-1/2}$ against λ when $\lambda = -1$, $\varphi = 0.01$, $\alpha = \beta = 0.1$

K	$C_{fx}\mathbf{Re}_x^{1/2}$		$\mathbf{Nu}_x\mathbf{Re}_x^{-1/2}$	
	Keller box (Present)	**bvp4c**	**Keller box (Present)**	**bvp4c**
0	0.76325636	0.7633	1.46043400	1.4604
	(−0.54691038)	(−0.5469)	(−0.63048561)	(−0.6305)
0.5	0.91490937	0.9149	1.4277145	1.4277
	(−0.58340852)	(−0.5828)	(−0.68278051)	(−0.6812)
1	1.0409512	1.0407	1.3988417	1.3987
	(−0.63798721)	(−0.6375)	(−0.72320866)	(−0.7220)

Note: Results shown in parentheses are the second solutions.

TABLE 5: Two-phase flow comparison of $1/(1-\varphi)^{2.5}F''(0)$ with results of Yacob et al. (2011) in the absence of other physical parameters

φ	**Cu**	$\mathbf{Al_2O_3}$	$\mathbf{TiO_2}$	**Present**		
				Cu	$\mathbf{Al_2O_3}$	$\mathbf{TiO_2}$
0.1	1.8843	1.6019	1.6192	1.8842	1.6021	1.6193
0.2	2.6226	2.0584	2.0942	2.6226	2.0583	2.0942

TABLE 6: Comparison of $F''(0)$ for different values of Pr in viscous fluid model when $\lambda = -1$ (for second solution)

Pr	**Ishak et al. (2008)**	**Present**
0.7	0.6917	0.6917
7	0.9235	0.9235
20	1.0031	1.0031
40	1.0459	1.0459
60	1.0677	1.0677
80	1.0817	1.0817
100	1.0918	1.0918

Figures 3(a)–3(c) show the impact of micropolar parameter K on the fluid velocity, microrotation profile, and temperature distribution, respectively. Figure 3(a) explains that the thickness of the velocity boundary layer becomes broader and broader due to K in both solutions. It is also clear that the velocity boundary layer is superior in the case of non-Newtonian fluid $(K \neq 0)$ compared to Newtonian fluid $(K = 0)$. Figure 3(b) indicates that the microrotation profile shrinks with rising K in first and second solutions. Physically, increasing the viscosity of microelements constantly encourages slow down in the flow nearby the surface. In contrast, the temperature distribution [Fig. 3(c)] increases with larger values of K in both solutions.

Figures 4(a)–4(c) are arranged to show the influence of porosity parameter α on the fluid velocity, microrotation profile, and temperature distribution. Figure 4(a) scrutinizes that the velocity rises due to growing values of α in the first solution, which consequently shrinks the velocity boundary layer. On the other hand, the opposite effect is observed in the second solution. As permeability of medium enhances, the regime grows to be further porous. Consequently, the force of Darcian body reduces. The Darcian resistance acts to slow down the particles of fluid in continua. This resistance moderates as permeability grows and therefore less progressively drag is acknowledged

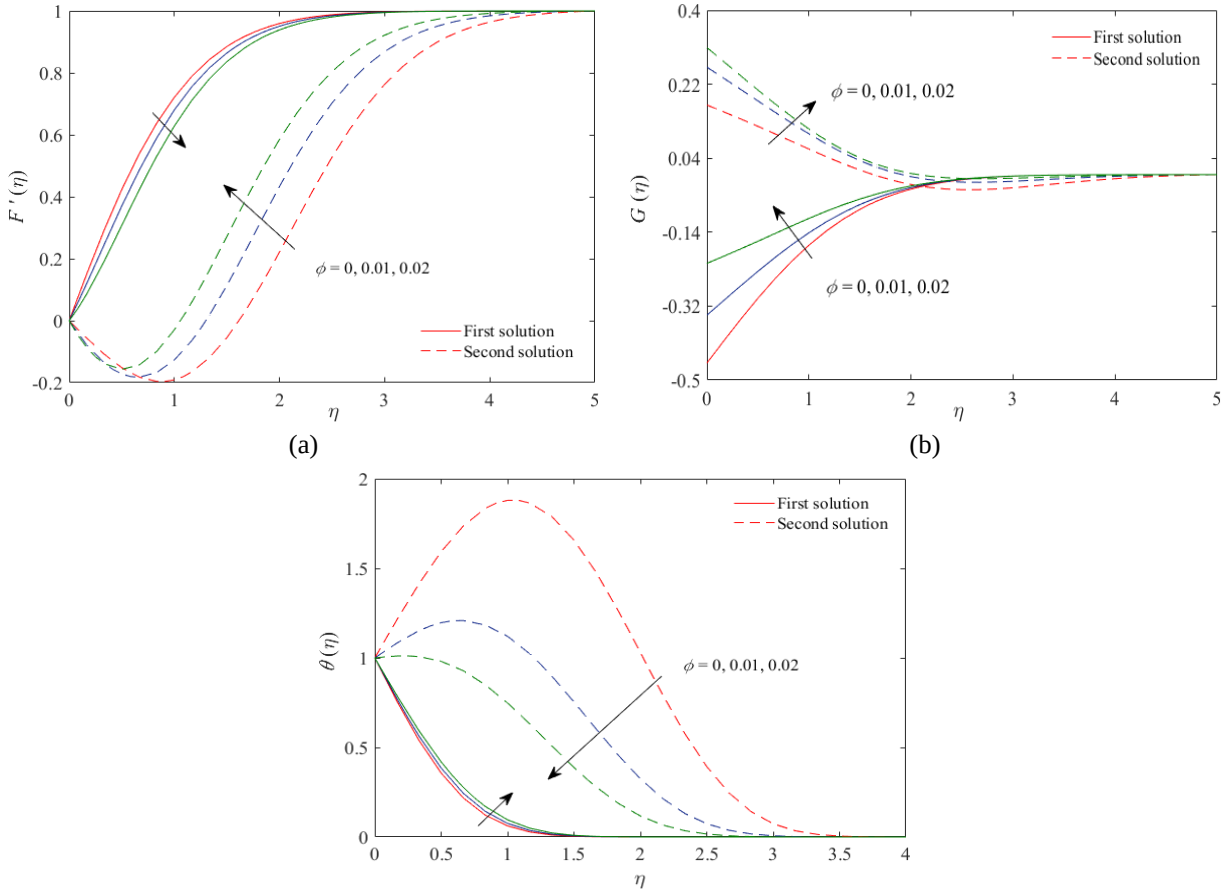

FIG. 2: Impact of φ on (a) $F'(\eta)$; (b) $G(\eta)$; and (c) $\theta(\eta)$ when $K = 0.2$, $M = 1$, $\lambda = -1$, and $\alpha = \beta = 0.03$

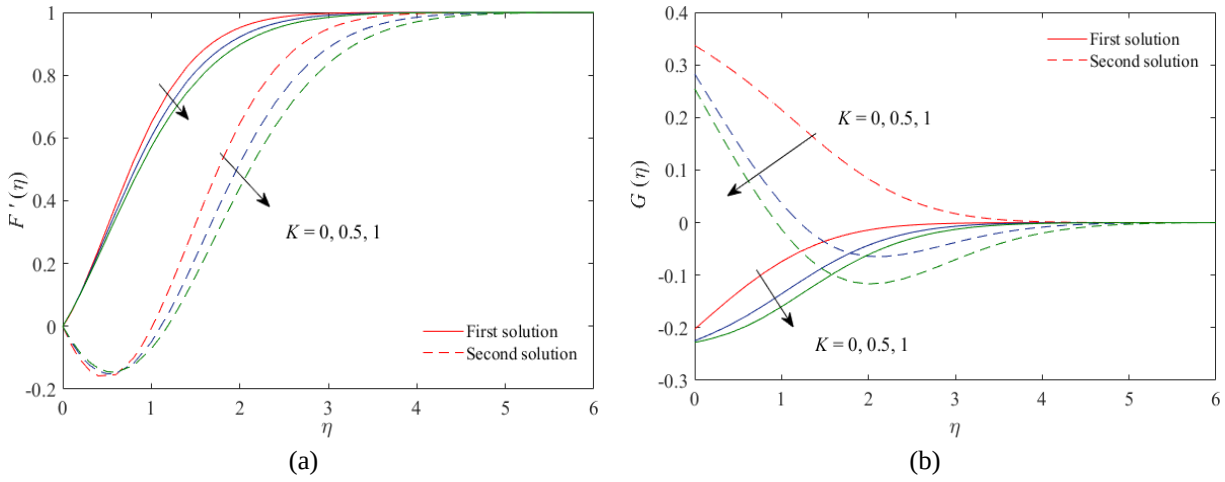

FIG. 3.

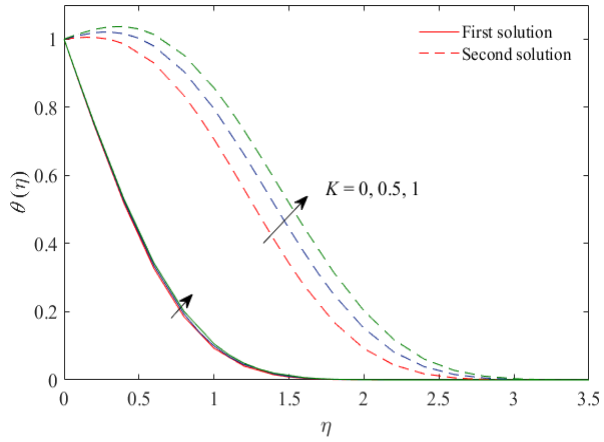

(c)

FIG. 3: Impact of K on (a) $F'(\eta)$; (b) $G(\eta)$; and (c) $\theta(\eta)$ when $\phi = 0.02$, $\alpha = \beta = 0.03$, and $\lambda = -1$

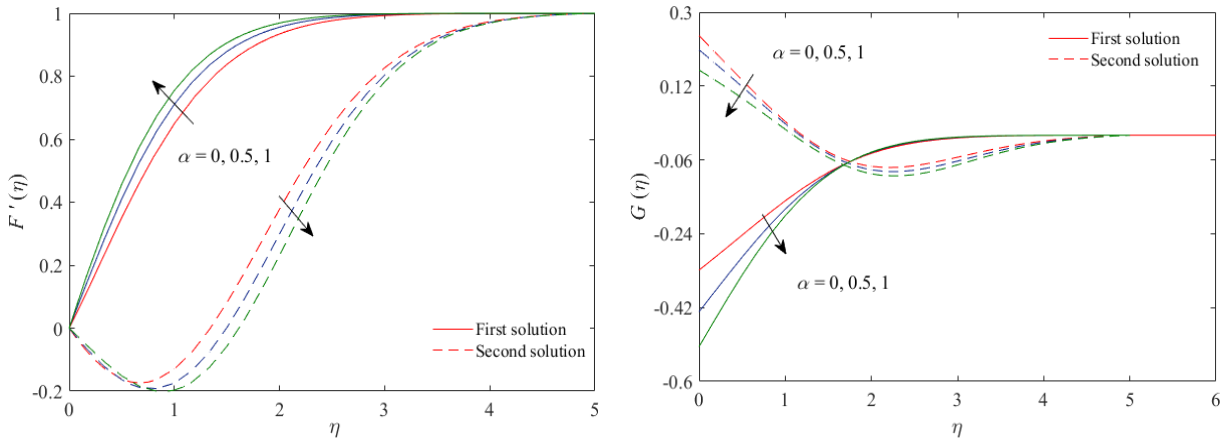

(a) (b)

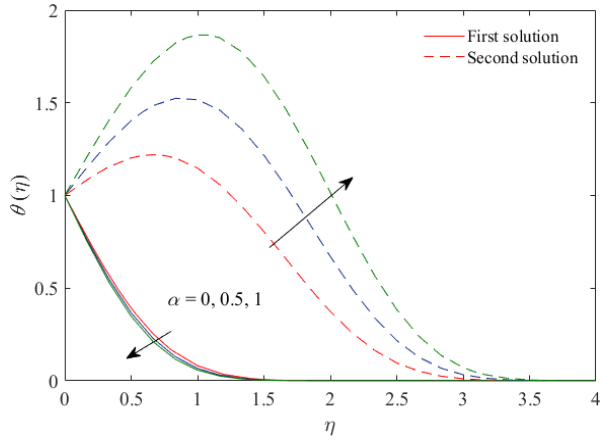

(c)

FIG. 4: Impact of α on (a) $F'(\eta)$; (b) $G(\eta)$; and (c) $\theta(\eta)$ when $\phi = 0.01$, $K = 0.5$, $\beta = 0.03$, and $\lambda = -1$

through the flow, and retardation of flow is thus declined. As a result, fluid velocity enhances as α increases in first solution. Figure 4(b) reveals that the microrotation profile confirms the decreasing behavior with growing values of α in both solutions, whereas Fig. 4(c) explains that the temperature distribution advances with bigger values of α in the second solution, whereas the reverse trend is captured in the first solution.

The impacts of inertia coefficient β on the fluid velocity, microrotation profile, and temperature distribution are presented in Figs. 5(a)–5(c), respectively. Figure 5(a) depicts that the fluid velocity increases due to β in the first solution, whereas the opposite tendency is watched in the second solution. Figure 5(b) suggests that the graph of microrotation shrinks with growing values of β in the first and second solutions. Temperature distribution [Fig. 5(c)] shows a decreasing trend with larger values of β in the first solution and increasing in the second solution. Therefore, the cooling rate is much quicker for larger values of the inertia parameter. It is also perceived that the thickness of the thermal boundary layer is larger in the second solution than the first solution.

The impacts of micropolar parameter, porosity parameter, inertia coefficient, Reynolds number, and Brinkman number on entropy generation are depicted in Figs. 6–10, respectively. Figure 6 elaborates that the entropy generation is climbing with micropolar parameter in both forms of solutions. It is also analyzed that the graph of entropy generation is superior in non-Newtonian fluid $(K \neq 0)$ compared to Newtonian fluid $(K = 0)$. Figures 7 and 8 reveal that due to porosity and inertia parameters, the entropy generation increases in both solutions. We observed from Figs. 9 and 10 that the profiles of entropy generation accelerates by either enhancing Reynolds or Brinkman numbers. Physically, the entropy produced from all irreversibility mechanisms and consequently, entropy enhances due

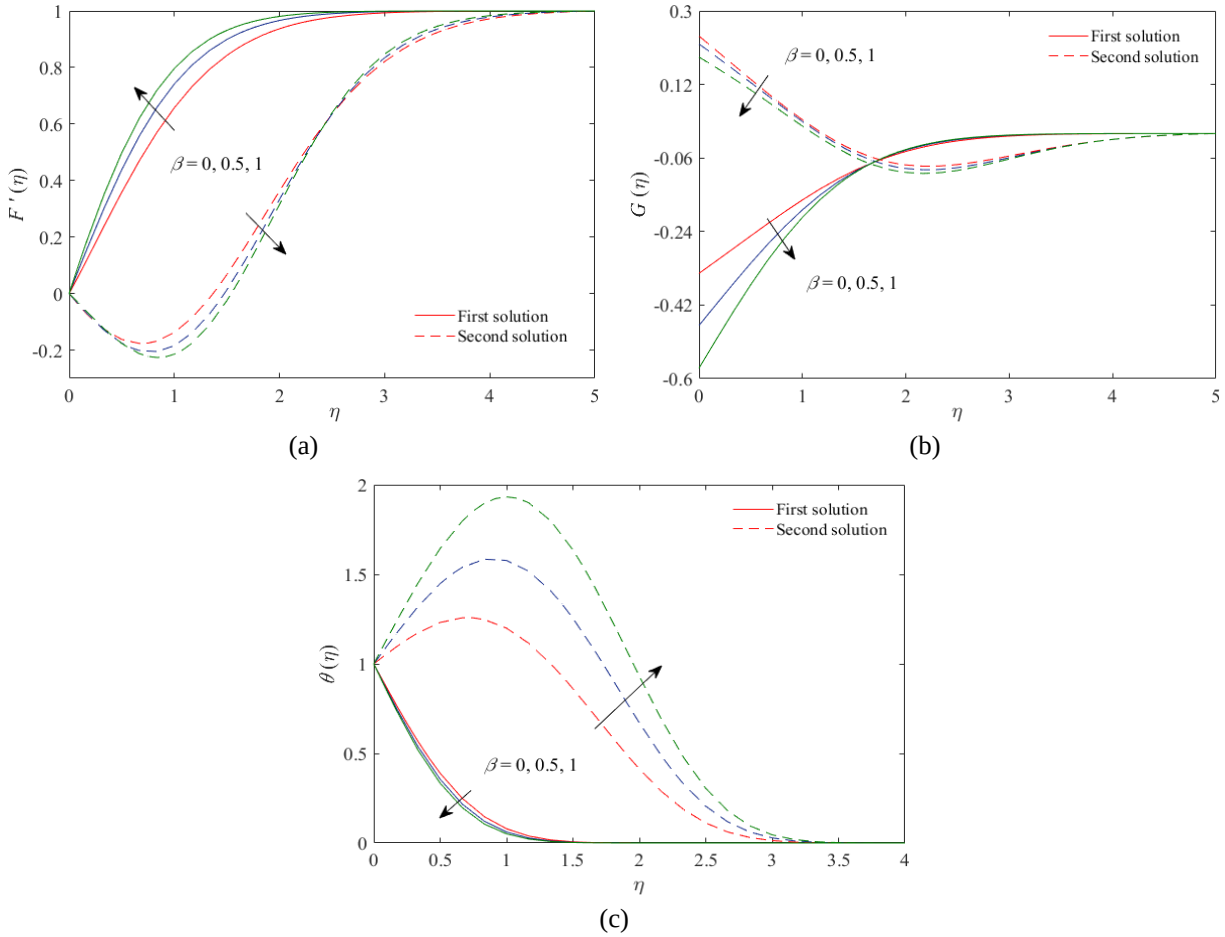

FIG. 5: Impact of β on (a) $F'(\eta)$; (b) $G(\eta)$; and (c) $\theta(\eta)$ when $\phi = 0.01$, $K = 0.5$, $\alpha = 0.1$, and $\lambda = -1$

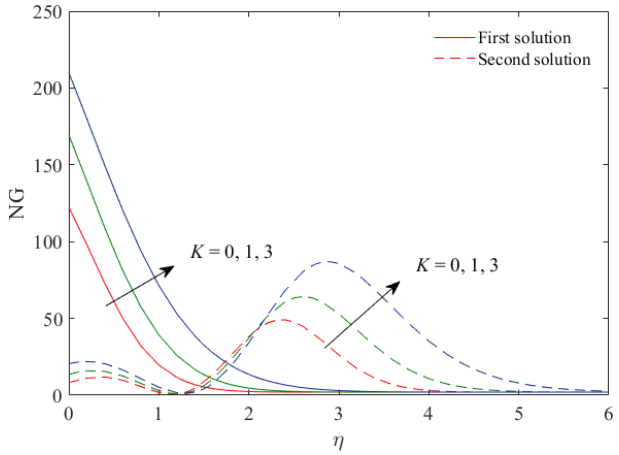

FIG. 6: Impact of K on NG when $\phi = 0.01$, $\lambda = -0.3$, $\alpha = \beta = 0.01$, $\mathrm{Re}_L = \mathrm{Br} = 1$, and $\Omega = 0.01$

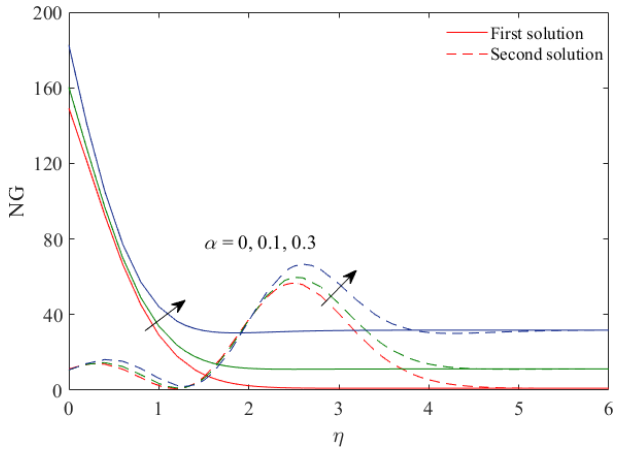

FIG. 7: Impact of α on NG when $\phi = 0.01$, $K = 0.5$, $\lambda = -0.3$, $\beta = 0.01$, $\mathrm{Re}_L = \mathrm{Br} = 1$, and $\Omega = 0.01$

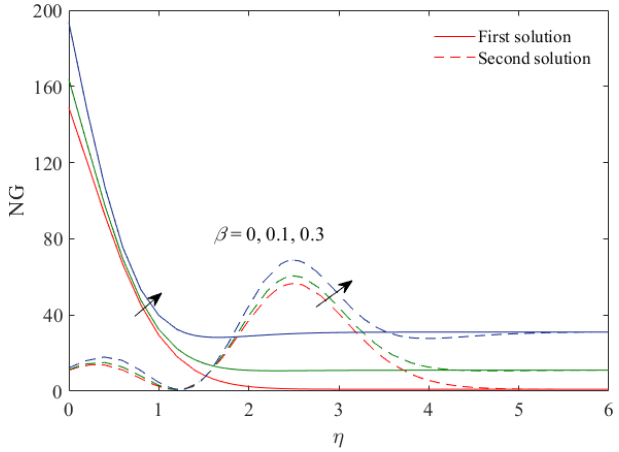

FIG. 8: Impact of β on NG when $\phi = 0.01$, $K = 0.5$, $\lambda = -0.3$, $\alpha = 0.01$, $\mathrm{Re}_L = \mathrm{Br} = 1$, and $\Omega = 0.01$

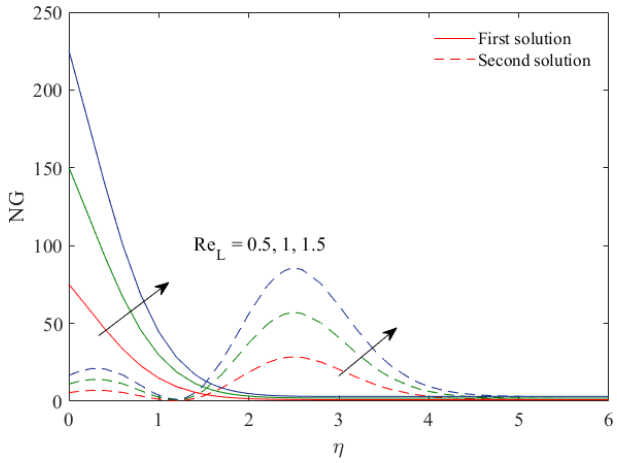

FIG. 9: Impact of Re_L on NG when $\phi = 0.01$, $K = 0.5$, $\lambda = -0.3$, $\alpha = \beta = 0.01$, Br = 1, and $\Omega = 0.01$

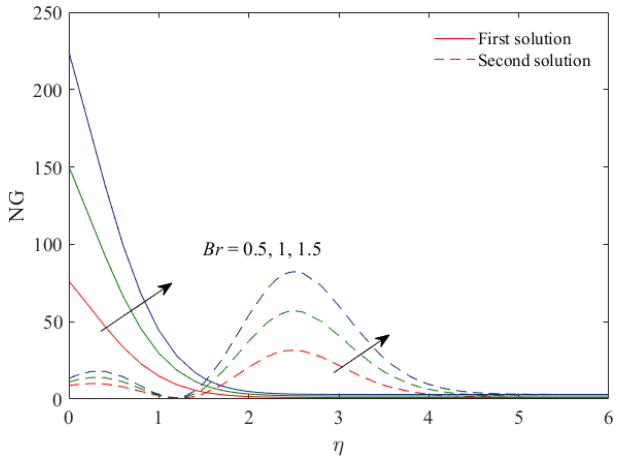

FIG. 10: Impact of Br on NG when $\phi = 0.01$, $K = 0.5$, $\lambda = -0.3$, $\alpha = \beta = 0.01$, $\mathrm{Re}_L = 1$, and $\Omega = 0.01$

to Reynolds number. Higher values of entropy generation generated through the fluid friction irreversibility happen owing to growing Brinkman number.

Figures 11(a) and 11(b) are presented to watch the performance of the skin friction and the Nusselt number against mixed convective parameter for preferred values of nanoparticle fraction. Multiple solutions are obtained for opposing flow, whereas a unique solution is found in assisting flow. The two different solutions were acquired by setting multiple guesses of η_∞, which generate two distinct profiles of velocity, microrotation, and temperature (Figs. 2 and 3) where these satisfy the conditions [Eq. (11)] asymptotically and therefore might not be ignored. The multiple results exist up to some critical values of λ (say λ_c), and no solution exists for $\lambda > \lambda_c$. At $\lambda = \lambda_c$, the solution is unique because branches of both solutions are connected. Based on computations, the values of λ_c are -4.2650, -2.4280, and -1.7190 for $\phi = 0$, 0.01, and 0.02, respectively. Thus the critical values decrease as nanoparticle fraction develops. Hence, the nanoparticle fraction accelerates the separation of boundary layer. Figures 11(a) and 11(b) indicate that the values of $C_{fx}\mathrm{Re}_x^{1/2}$ and $\mathrm{Nu}_x\mathrm{Re}_x^{-1/2}$ initially increase and then reduce as φ increases in both solutions. Moreover, it is clear that all profiles intersect $\lambda = 0$ (buoyancy force absent). Since Eqs. (8) and (10) are decoupled when $\lambda = 0$. It is also explored from these figures that the values of $C_{fx}\mathrm{Re}_x^{1/2}$ and $\mathrm{Nu}_x\mathrm{Re}_x^{-1/2}$climb as mixed parameter enhances in case of assisting flow, whereas in opposing flow, the reverse trend is noticed. Physically, a favorable pressure gradient produces by assisting flow, which improves the motion of fluid, which consecutively

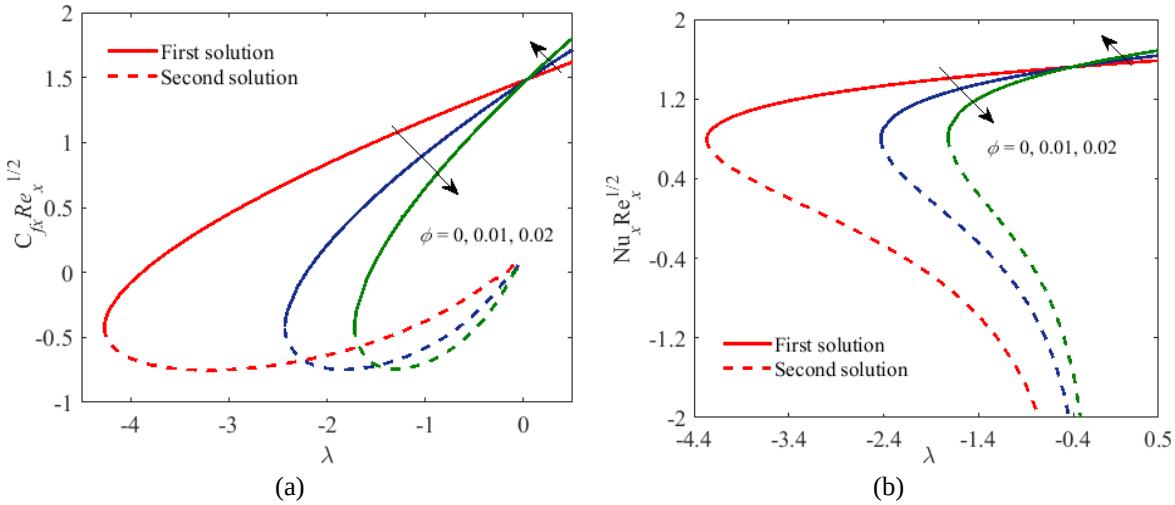

FIG. 11: Impact of φ on (a) $C_{fx}\mathrm{Re}_x^{1/2}$; and (b) $\mathrm{Nu}_x\mathrm{Re}_x^{-1/2}$ when $K = 0.5$, $\alpha = \beta = 0.1$

enhances the rate of heat transfer and surface shear stress at the plate. In contrast, opposing flow guides an unfavorable pressure gradient which delays the flow, and thus $C_{fx}\mathrm{Re}_x^{1/2}$ and $\mathrm{Nu}_x\mathrm{Re}_x^{-1/2}$ decrease.

Figures 12(a) and 12(b) show the influence of micropolar parameter on $C_{fx}\mathrm{Re}_x^{1/2}$ and $\mathrm{Nu}_x\mathrm{Re}_x^{-1/2}$ against λ. The values of $C_{fx}\mathrm{Re}_x^{1/2}$ lift due to enhancing K in the first solution and turn down in the second solution. Figure 12(b) shows that the values of $\mathrm{Nu}_x\mathrm{Re}_x^{-1/2}$ decompose initially and then after certain value of λ, it's starting to increase as K progresses. Based on calculations, the values of λ_c are -2.2830, -2.4280, and -2.5350 for $K = 0$, 0.5, and 1, respectively. Thus the critical values increase as K expands. Hence, the micropolar parameter delays the separation of boundary layer.

Figures 13(a) and 13(b) show the patterns of streamlines for first and second solutions. Figure 13(a) signifies that the streamlines are symmetric, simple, and fuller toward an axis in the first solution because of equal forces of assisting and opposing flows. Alternatively, streamlines are slightly complicated in the second solution and separated the flows in double region as shown in Fig. 13(b).

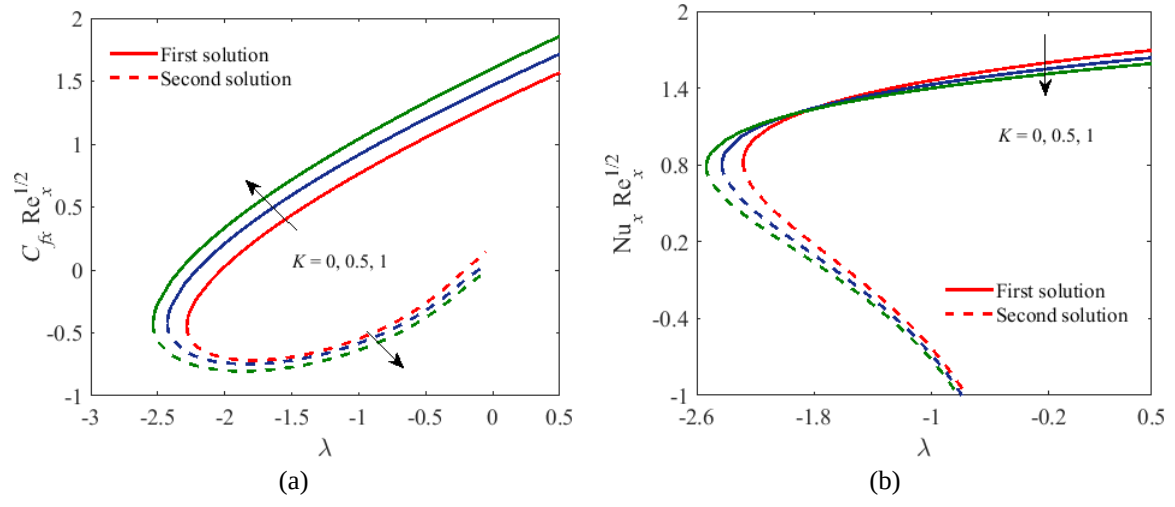

FIG. 12: Impact of K on (a) $C_{fx}\mathrm{Re}_x^{1/2}$; and (b) $\mathrm{Nu}_x\mathrm{Re}_x^{-1/2}$ when $\varphi = 0.01$, $\alpha = \beta = 0.1$

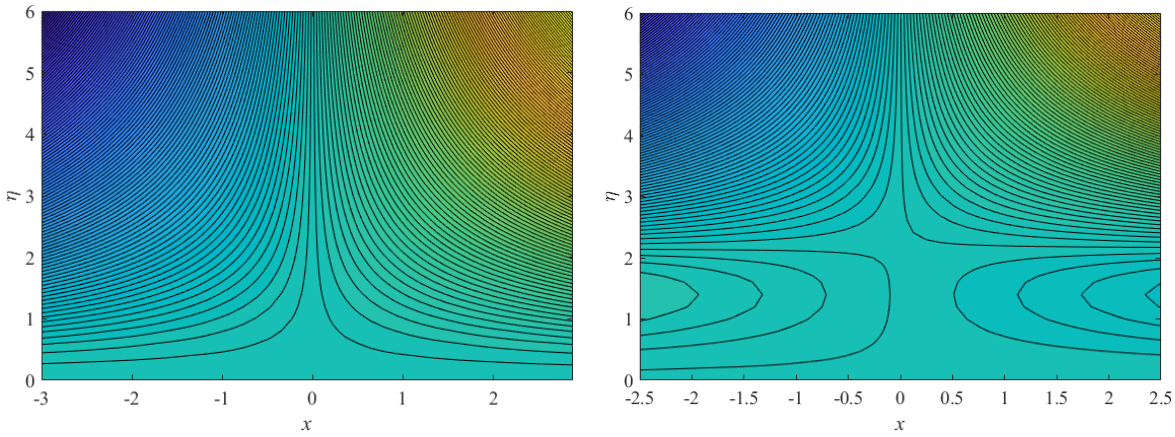

FIG. 13: Streamlines (a) first solution; and (b) second solution when $K = 0.5$, $\phi = 0.01$, $\alpha = \beta = 0.1$, and $\lambda = -0.1$

4. FINAL REMARKS

In the present inspection, the impact of entropy generation on mixed convective flow of micropolar fluid composed of water-based TiO_2 nanomaterial toward a vertical plate embedded in non-Darcy porous medium has been investigated. Similarity transformations have been applied to model the governing flow problem. The results of the governing flow problem are achieved through the Keller box technique. The important outcomes for the current analysis are as follows:

- Multiple solutions are obtained for opposing flow, while the unique solution is obtained for assisting flow.
- The velocity of fluid decreases due to φ in the first solution and increases in the second solution, while conflicting performance is seen on temperature distribution. However, microrotation profile increases in the first solution and the second solution.
- Micropolar parameter decreases the velocity of fluid and microrotation in the first and second solutions and leads to increase the temperature distribution in the first and second solutions.
- Velocity boundary layer shrinks due to porous and inertia parameters in the first solution, whereas the opposite observations are perceived in the second solution. Microrotation profile depicts the declining behavior in both solutions. Temperature distribution decreases in the first solution and increases in the second solution due to porous and inertia parameters.
- The separation of boundary layer accelerates due to volume fraction and delays due to micropolar parameter.
- Profiles of entropy generation enhance due to micropolar, porosity, inertia and parameters, as well as the Reynolds and Brinkman numbers.
- The value of skin friction rises due to micropolar fluid in the case of the first solution, whereas the reverse trend was noticed in the case of the second solution. On the other hand, the Nusselt number decreases due to micropolar fluid in both solutions.
- Due to volume fraction, the skin friction and the Nusselt number initially increase and then decrease after a certain value of volume fraction.
- Streamlines are fuller, symmetric, and quite simple toward an axis in the first solution, and streamlines are slightly complicated and split the flow in two regions in the second solution.

ACKNOWLEDGMENT

We thankfully acknowledge the referees for their helpful observations, which enhanced the features of the paper.

REFERENCES

Aman, F., Ishak, A., and Pop, I., Mixed Convection Boundary Layer Flow near Stagnation-Point on Vertical Surface with Slip, *Appl. Math. Mech. Eng. E*, vol. **32**, no. 12, pp. 1599–1606, 2011.

Bakar, S.A., Arifin, N.M., Nazar, R., Ali, F.M., Bachok, N., and Pop, I., The Effects of Suction on Forced Convection Boundary Layer Stagnation Point Slip Flow in a Darcy Porous Medium towards a Shrinking Sheet with Presence of Thermal Radiation: A Stability Analysis, *J. Porous Media*, vol. **21**, no. 7, pp. 623–636, 2018.

Butt, A.S. and Ali, A., Entropy Analysis of Magnetohydrodynamic Flow and Heat Transfer over a Convectively Heated Radially Stretching Surface, *J. Taiwan Inst. Chem. Eng*., vol. **45**, pp. 1197–1203, 2014.

Choi, S.U.S., Enhancing Thermal Conductivity of Fluids with Nanoparticle, *ASME Fluids Eng. Div*., vol. **231**, pp. 99–105, 1995.

Das, K. and Duari, P.R., Micropolar Nanofluid Flow over a Stretching Sheet with Chemical Reaction, *Int. J. Appl. Comput. Math*., vol. **3**, pp. 3229–3239, 2017.

Eringen, A.C. Theory of Micropolar Fluids, *J. Appl. Math. Mech*., vol. **16**, pp. 1–18, 1966.

Gireesha, B.J., Mahanthesh, B., Manjunatha, P.T., and Gorla, R.S.R., Numerical Solution for Hydromagnetic Boundary Layer Flow and Heat Transfer past a Stretching Surface Embedded in Non-Darcy Porous Medium with Fluid-Particle Suspension, *J. Nigerian Math. Soc*., vol. **34**, pp. 267–285, 2015.

Hayat, T., Nazar, H., Imtiaz, M., and Alsaedi, A., Darcy–Forchheimer Flows of Copper and Silver Water Nanofluids between Two Rotating Stretchable Disks, *Appl. Math. Mech. Eng. Ed*., vol. **38**, no. 12, pp. 1663–1678, 2017.

Hsiao, K.L., Micropolar Nanofluid Flow with MHD and Viscous Dissipation Effects towards a Stretching Sheet with Multimedia Feature, *Int. J. Heat Mass Transf*., vol. **112**, pp. 983–990, 2017.

Hussanan, A., Salleh, M.Z., and Khan, I., Microstructure and Inertial Characteristics of a Magnetite Ferrofluid over a Stretching/Shrinking Sheet Using Effective Thermal Conductivity Model, *J. Mol. Liq*., vol. **255**, pp. 64–75, 2018.

Hussanan, A., Salleh, M.Z., Khan, I., and Tahar, R.M., Unsteady Free Convection Flow of a Micropolar Fluid with Newtonian Heating: Closed Form Solution, *Therm. Sci*., vol. **21**, pp. 2313–2326, 2017.

Iqbal, Z., Ahmed, B., and Miraj, E., A Numerical Study of Ferrofluid in Presence of Magnetic Dipole Inspired by Slip and Viscous Dissipation Effects Submerged in Porous Medium, *J. Porous Media*, vol. **22**, no. 1, pp. 107–117, 2019.

Ishak, A., Nazar, R., and Pop, I., Post-Stagnation-Point Boundary Layer Flow and Mixed Convection Heat Transfer over a Vertical, Linearly Stretching Sheet, *Arch. Mech*., vol. **60**, no. 4, pp. 303–322, 2008.

Khan, M.I., Hayat, T., Qayyum, S., Khan, M.I., and Alsaedi, A., Entropy Generation (Irreversibility) Associated with Flow and Heat Transport Mechanism in Sisko Nanomaterial, *Phys. Lett. A*, vol. **382**, no. 34, pp. 2343–2353, 2018.

Khan, W.A. and Pop, I., Boundary-Layer Flow of a Nanofluid past a Stretching Sheet, *Int. J. Heat Mass Transf*., vol. **53**, pp. 2477–2483, 2010.

Lok, Y.Y., Amin, N., and Pop, I., Unsteady Mixed Convection Flow of a Micropolar Fluid near the Stagnation-Point on a Vertical Surface, *Int. J. Therm. Sci*., vol. **45**, no. 12, pp. 1149–1157, 2006.

Mabood, F., Ibrahim, S.M., Rashidi, M.M., Shadloo, M.S., and Lorenzini, G., Non-Uniform Heat Source/Sink and Soret Effects on MHD Non-Darcian Convective Flow past a Stretching Sheet in a Micropolar Fluid with Radiation, *Int. J. Heat Mass Transf*., vol. **93**, pp. 674–682, 2016.

Makinde, O.D. and Aziz, A., Boundary Layer Flow of a Nanofluid past a Stretching Sheet with a Convective Boundary Condition, *Int. J. Therm. Sci*., vol. **50**, pp. 1326–1332, 2011.

Makinde, O.D., Mabood, F., Khan, W.A., and Tshehla, M.S., MHD Flow of a Variable Viscosity Nanofluid over a Radially Stretching Convective Surface with Radiative Heat, *J. Mol. Liq*., vol. **219**, pp. 624–630, 2016.

Mukhopadhyay, S., De, P.R., Bhattacharyya, K., and Layek, G.C., Forced Convective Flow and Heat Transfer over a Porous Plate in a Darcy–Forchheimer Porous Medium in Presence of Radiation, *Meccanica*, vol. **47**, pp. 153–161, 2012.

Prasad, V.R., Gaffar, S.A., Reddy, E.K., and Beg, O.A., Numerical Study of Non-Newtonian Boundary Layer Flow of Jeffreys

Fluid past a Vertical Porous Plate in a Non-Darcy Porous Medium, *Int. J. Comp. Meth. Eng. Sci. Mech*., vol. **15**, pp. 372–389, 2014.

Rashid, I., Haq, R.U., Khan, Z.H., and Al-Mdallal, Q.M., Flow of Water based Alumina and Copper Nanoparticles along a Moving Surface with Variable Temperature, *J. Mol. Liq*., vol. **246**, pp. 354–362, 2017.

Saleh, S.H.M., Arifin, N.M., Nazar, R., and Pop, I., Unsteady Micropolar Fluid over a Permeable Curved Stretching Shrinking Surface, *Math. Prob. Eng*., vol. **2017**, pp. 1–13, 2017.

Sandeep, N., Sulochana, C., Raju, C.S.K., Babu, M.J., and Sugunamma, V., Unsteady Boundary Layer Flow of Thermophoretic MHD Nanofluid past a Stretching Sheet with Space and Time Dependent Internal Heat Source/Sink, *Appl. Appl. Math*., vol. **10**, no. 1, pp. 312–327, 2015.

Shateyi, S., Motsa, S.S., and Makukula, Z., On Spectral Relaxation Method for Entropy Generation on a MHD Flow and Heat Transfer of a Maxwell Fluid, *J. App. Fluid Mech*., vol. **8**, pp. 21–31, 2015.

Spasojević, M.D., Janković, M.R., and Djaković, D.D., A New Approach to Entropy Production Minimization in Diabatic Distillation Column with Trays, *Therm. Sci*., vol. **14**, pp. 317–328, 2010.

Sreenadh, S., Krishna, G.G., Srinivas, A.N.S., and Sudhakara, E., Entropy Generation Analysis for MHD Flow through a Vertical Deformable Porous Layer, *J. Porous Media*, vol. **21**, no. 6, pp. 523–538, 2018.

Umavathi, J.C. and Sasso, M., Free Convection Flow in a Duct Filled with Nanofluid and Saturated with Porous Medium: Variable Properties, *J. Porous Media*, vol. **21**, no. 1, pp. 1–33, 2018.

Wang, X., Xu, X., and Choi, S.U.S., Thermal Conductivity of Nanoparticle Fluid Mixture, *J. Thermophys., Heat Transf*., vol. **13**, pp. 474–480, 1999.

Waqas, H., Hussain, S., Sharif, H., and Khalid, S., MHD Forced Convective Flow of Micropolar Fluids past a Moving Boundary Surface with Prescribed Heat Flux and Radiation, *British J. Math. Comput. Sci*., vol. **21**, no. 1, pp. 1–14, 2017.

Yacob, N.A., Ishak, A., and Pop, I., Falkner-Skan Problem for a Static or Moving Wedge in Nanofluids, *Int. J. Therm. Sci.*, vol. **50**, no. 2, pp. 133–139, 2011.

Yasmin, A., Ali, K., Ghaffar, M., and Ashraf, M., On Viscous Dissipation and Thermal Characteristics of Magnetohydrodyanics Micropolar Fluid Flow in Porous Channel with Expanding or Contracting Walls, *J. Porous Media*, vol. **22**, no. 2, pp. 243–260, 2019.

Zaib, A., Rashidi, M.M., and Chamkha, A.J., Flow of Nanofluid Containing Gyrotactic Microorganisms over a Static Wedge in Darcy-Brinkman Porous Medium with Convective Boundary Condition, *J. Porous Media*, vol. **21**, no. 10, pp. 911–928, 2018.

Zaib, A., Rashidi, M.M., Chamkha, A.J., and Bhattacharyya, K., Numerical Solution of Second Law Analysis for MHD Casson Nanofluid past a Wedge with Activation Energy and Binary Chemical Reaction, *Int. J. Num. Meth. Heat Fluid Flow*, vol. **27**, no. 12, pp. 2816–2834, 2017.